Eur. Phys. J. D **23**, 223–228 (2003)
DOI: 10.1140/epjd/e2003-00058-0

THE EUROPEAN PHYSICAL JOURNAL D

# Measurementof the $4s^2\ {}^1S_0 \longrightarrow 4s3d\ {}^1D_2$ transition probability in calcium

N. Beverini[1,a], E. Maccioni[1], F. Sorrentino[1], V. Baraulia[2], and M. Coca[1]

[1] Istituto Nazionale per la Fisica della Materia and Dipartimento di Fisica "E. Fermi", via F. Buonarroti 2, 56127 Pisa, Italy
[2] Institute of Laser Physics, Russian Academy of Sciences, Pr. Lavrenteva 13/3, 630090 Novosibirsk, Russia

Received 17 June 2002 / Received in final form 9 December 2002
Published online 4 March 2003 – 

**Abstract.** We have measured the ratio between the transition probabilities of two forbidden lines in Ca: the intercombination line at 657.3 nm and the $E2$ line at 457.5 nm. The value we obtained for this ratio is $(54.1 \pm 2.4)$. Combined with the most accurate value available in literature for the lifetime of the $^3P_1$ level, our measurement gives a value of $(54.4 \pm 4.0)$ s$^{-1}$ for the $^1S_0 \rightarrow {}^1D_2$ transition probability, significantly more accurate than the previous determinations.

**PACS.** 32.30.-r Atomic spectra – 32.70.Cs Oscillator strengths, lifetimes, transition moments – 42.62.Fi Laser spectroscopy

## 1 Introduction

The forbidden transitions between the ground state and the metastable levels of calcium and magnesium have a large metrological interest for frequency standards in the visible and near-infrared regions. Much work has been done on the calcium $^1S_0 \rightarrow {}^3P_1$ intercombination line at 657.3 nm [1–4], and some works are in progress on the corresponding $^1S_0 \rightarrow {}^3P_1$ transition in magnesium at 457.1 nm [5,6].

The $^1S_0 \rightarrow {}^1D_2$ transition in calcium (Fig. 1) seems very attractive too, due to its narrow natural line-width (<10 Hz). The $^1D_2$ metastable level can be excited either through an electrical quadrupole absorption at 457.5 nm ($E2$ line), or through a dipole-allowed two-photon absorption at 915 nm. In particular the two-photon transition appears interesting for metrological applications, because of its intrinsic Doppler-free properties, and an experiment is now in progress in our laboratory to observe it on a cooled and trapped sample of calcium atoms.

In this paper we present a measurement of the $4s^2\ {}^1S_0 \rightarrow 4s3d\ {}^1D_2$ $E2$ transition probability. In the literature there are some data on the $^1D_2$ level lifetime [7], which is however dominated by the $^1D_2 \rightarrow {}^3P_1$ decay. The only experimental value available in literature for the $E2$ transition rate has a large error (20%, see [8]), and the theoretical estimations are not univocal. The multiconfiguration self-consistent-field + configuration interaction (MCSCF/CI) calculations [9,10] using Slater-type orbitals gave values around $80 \div 90$ s$^{-1}$ by taking only valence correlation into account. The effect of core-valence correlation was included in an "all electron" CI calculation [11], using extended Gaussian-type orbitals. In this frame, the core-valence correlation reduces the transition rate by 44%, leading to a value (39.6 s$^{-1}$) in perfect agreement with the experimental result of reference [8]. On the other hand, a different approach to core-valence correlation by way of first-order theory of oscillator strength (FOTOS) had lead to a smaller reduction (15%) of the transition rate [12]. The two-electron multiconfiguration Hartree-Fock (MCHF) calculation by Vaeck *et al.* [13] gave again a value higher than 70 s$^{-1}$. Recently a value of 48.1 s$^{-1}$ was obtained using a fully relativistic multiconfiguration Dirac-Fock method with Breit and QED

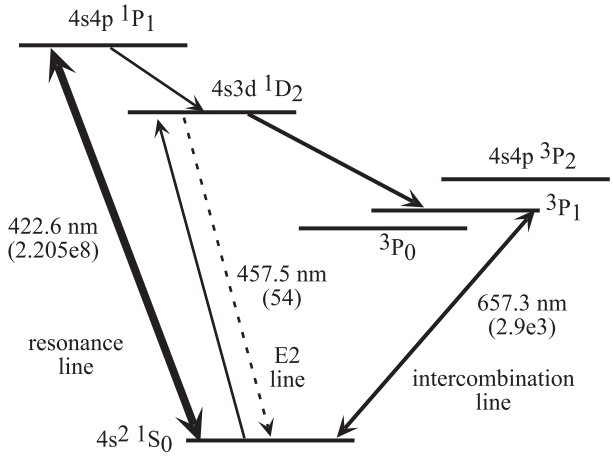


**Fig. 1.** Ca energy levels; the numbers in parentheses are the transition rates in s$^{-1}$.

[a] e-mail: beverini@df.unipi.it

**Table 1.** Values for the $E2$ transition probability in $s^{-1}$. $L$: length representation; $V$: velocity representation.

| reference and year | theoretical values $L$ | $V$ | experimental values |
|---|---|---|---|
| [9] 1980 | 87 | 116 | |
| [8] 1982 | | | $40 \pm 8$ |
| [10] 1981 | 81 | | |
| [11] 1985 | 39.6 | | |
| [12] 1983 | 60.2 | 65.9 | |
| [13] 1991 | 70.5 | 78.3 | |
| [14] 2001 | 48.1 | | |
| this work | | | $54.4 \pm 4.0$ |

corrections [14], but details about the calculations are not available. The situation is summarized in Table 1.

In our experiment the $E2$ transition probability was measured by monitoring the transmission of a 50 cm long absorption cell that has been specially designed in order to work at a calcium vapor density of some $10^{15}$ $cm^{-3}$ (corresponding to 650–700 °C). The radiation at 457.5 nm was generated by frequency doubling in a $KNbO_3$ crystal the output of a CW tunable Ti:Sa laser, which can operate single-mode at the wavelength of 915 nm. The effective density in the cell was calibrated by measuring the absorption on the $^1S_0 \rightarrow {}^3P_1$ intercombination line at 657.3 nm, whose transition probability is well known from the literature [15]. The source for the radiation at 657.3 nm was a diode laser in an extended cavity.

## 2 Experimental apparatus

A sketch of the experimental apparatus is shown in Figure 2. It is essentially made up of the two laser sources, tunable around 657.3 nm and 915 nm respectively, a SHG system providing the radiation at 457.5 nm, the absorption cell and a data acquisition system, which provides the normalization of the laser intensities and the frequency scale linearization during the sweeps.

The cell transmission for the two laser beams was monitored through photodiodes 1 and 2; a small fraction of radiation was split from the beams just before passing the cell, and detected through photodiodes 3 and 4 for monitoring the intensity of the lasers. The calibration of the frequency scale during the sweeps was provided by two Fabry-Pérot interferometers. The effective absorption length for the $E2$ transition was increased by a factor of three, using a three-pass geometry.

### 2.1 The Ti:Sa laser

The blue radiation at 457.5 nm was generated through SHG of the 915 nm wavelength coming from a home-made Ti:Sa laser. All the elements of this IR laser are mounted on an optical breadboard (isolated from the table with rubber feet) by means of small magnetic bases. The

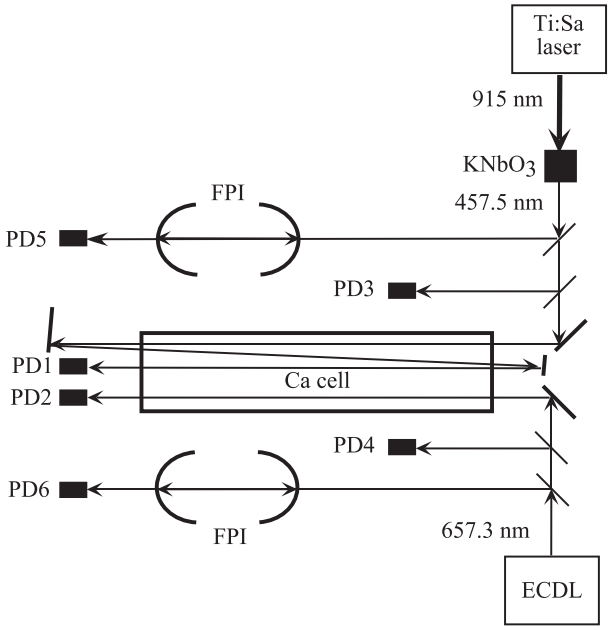


**Fig. 2.** Schematic of the experiment. ECDL: extended cavity diode laser; PD: photodiode; FPI: Fabry-Pérot interferometer.

non-planar ring cavity is made of two spherical mirrors (curvature radius 15 cm) and four plane mirrors. Halfway between the concave mirrors a 20 mm long, Brewster-cut, Ti:Sa crystal is positioned. The laser is pumped by a commercial green Nd:YVO laser system capable of 10 W of power at 532 nm.

The unidirectional device is formed by a Faraday rotator and a system of three mirrors. One of these mirrors is out of the plane of the laser cavity, so that the resulting reflection from the optical system generates a rotation of the polarization of the laser beam which compensates for the polarization angular displacement induced by the Faraday rotator [16].

Three intra-cavity elements are used to obtain single frequency operation: a three-plates birefringent filter, a thin etalon and an air-spaced tunable thick etalon, made of two separate prisms, whose relative distance is controlled by a PZT element. Two of the plane mirrors are mounted on PZT translation systems to allow the tuning of the optical length of the laser cavity (free spectral range about 240 MHz). One of these two mirrors constitutes the output coupler of the system, with a transmission of about 5.5% around 915 nm. The single-frequency output power at this wavelength is about 400 mW, with a pump power of 9 W. In order to prevent cavity mode jumps during the frequency scanning, a servo circuit locks the transmission maximum of the thick etalon to the laser cavity length. In this way we obtain a continuous frequency scan of about 3 GHz, where the limitation is imposed by the maximum allowed stretching of the PZTs of the cavity mirrors. During our measurements, no frequency stabilization has been provided to the Ti:Sa laser; the bandwidth of the laser mode is about 10 MHz (frequency jitter), as checked by an external Fabry-Pérot spectrum analyser.

### 2.2 Second harmonic generation (SHG)

The fundamental radiation at 915 nm, generated by the CW Ti:Sa laser, was frequency doubled in a single-pass through a temperature tuned $KNbO_3$ non-linear crystal [17,18], in a condition of non-critical phase-matching. For this purpose the IR light beam was focused by an AR coated lens ($f = 10$ cm) onto the 10 mm long crystal, positioned in a temperature-controlled oven. The right temperature for SHG at this wavelength is about 140 °C: this value was fixed and kept constant at the level of few mK by means of a servo loop, with a Peltier module as a heater and a thermistor as a temperature probe. The crystal we used had an AR coating which was optimized on a slightly different wavelength. Anyway we obtained about 300 $\mu$W of blue light, suitable for the absorption experiment. No attempt was made in order to optimize the SHG efficiency, as the available power was largely enough for our purposes.

The radiation at 457.5 nm was separated from the IR beam with the help of a coloured glass filter. Finally it was collimated in a diameter of about 2 mm, and sent through the calcium cell.

### 2.3 The 657.3 nm laser source

The 657.3 nm laser source is an Extended Cavity Diode Laser (ECDL) mounted in the Littrow configuration [19,20]. It consists of a 30 mW commercial red diode laser (whose thin glass window has been removed) optically coupled to a 1800 lines/mm holographic grating. The first diffraction order from this wavelength selective element is sent back to the diode. This optical feedback technique is employed for narrowing the emission line-width and for obtaining a broad tuning of the emission wavelength without mode jumps. The laser frequency can be swept around the atomic resonance by tuning the cavity length through a PZT mounted on the grating. The output radiation is obtained as the zero order of diffraction from the grating. The typical performance of our ECDL is a CW-output power of 8–10 mW (single mode, with a rms-bandwidth of about 1 MHz) and a continuous frequency scan up to about 6 GHz. Rotation of the grating during the frequency sweep causes a very small misalignment of the laser beam (displacement less than 0.1 mm at 3 m far from the source).

### 2.4 Frequency calibration system

In order to provide a calibrated scale for the frequency scanning (more than 5 GHz wide) of the two lasers, a small fraction of each beam was sent into high-finesse Fabry-Pérot resonators. The free spectral range of the two resonators is $300 \pm 1$ MHz and $298 \pm 1$ MHz, for the red and the blue beams respectively. We linearized the frequency scales by performing a polynomial fit on the position of the transmission peaks from the interferometers.

### 2.5 The calcium absorption cell

The cell has been designed to reach a calcium vapor pressure high enough to have a significant absorption on the weak blue quadrupole transition. In order to avoid the unpractical use of very long cells, we heated the absorption cell up to 650–700 °C to have atomic densities greater than $10^{15}/cm^3$. In this way, with a three-pass geometry for the blue light beam, we were able to measure peak absorptions of $10 \div 15\%$, with a signal to noise ratio larger than 200. The corresponding peak absorption on the red intercombination line was about $96 \div 99\%$ (single-pass). The cell is made of a 50 cm long steel pipe with a diameter of 2.5 cm. At its center a small calcium reservoir is soldered to the pipe. A coaxial resistive wire (thermocoax) is anti-inductively wrapped around the principal cylinder, leaving out the reservoir. This defines the coldest point of the oven, whose temperature is checked by means of a thermocouple. A second thermocouple is positioned on the body of the pipe, while a third one is located on one end. The resistive wire is tightened to the body of the principal pipe by two semi-cylindrical steel parts, kept together by small steel bands. The structure is then housed inside another steel pipe, which works as a heat shield. This system of two concentric pipes is put inside a larger steel vacuum cylinder, with a port for the mechanical pump connection and a feedthrough for current and thermocouples. The vacuum chamber is closed by two water cooled ISO 100 flanges, supporting the housings for the output Pyrex windows, mounted at the Brewster angle with respect to the linear polarization of the blue light (laying in the vertical plane). On the pump port there is a two-way valve that allows one to fill the cell with $10 \div 20$ Pa of Ar. The presence of the buffer gas is fundamental to confine the calcium vapor inside the tube and to prevent condensation on the windows. The chosen pressure is low enough to avoid perturbations of the line profile. In fact, the pressure-broadening coefficient for Ar–Ca interaction is about 150 kHz/Pa for the intercombination line [21] and about 100 kHz/Pa for the $E2$ line [8], against a Doppler line-width of about 2 GHz at 650 °C. The structure of our cell is quite simpler than a conventional heat-pipe, and it was adequate for our purpose.

### 2.6 Data acquisition system

A computer collected the signals coming from the six Si photodiodes *via* an ADC 12-bit board. We chose an integration time of 5 ms for the photodiodes 1, 2, 3 and 4 (Fig. 2). The frequencies of the two lasers were simultaneously scanned, and the scan duration was about 8 seconds. The readings from the thermocouples were acquired too, and we waited until they were stable enough before storing a set of measures, in order to be sure that the cell was in stationary conditions.

## 3 Data analysis

With our apparatus we measured the ratio between the transition probabilities of the intercombination line and

the $E2$ line. As the transition rate of the intercombination line is already known by lifetime measurements of the $^3P_1$ level, we could estimate the transition rate of the $E2$ line with an accuracy which is limited by the uncertainty on the $^3P_1$ lifetime value.

The value of the ratio between the transition rates was obtained by comparing the integral of the absorption coefficient $\alpha(\nu, x)$ on the two lines. The absorption coefficient depends on the atomic density $N(x)$ and on the transition rate $\mathcal{A}_{ki}$ as

$$\alpha(\nu, x) = N(x)\frac{g_k}{g_i}\frac{\lambda^2}{4\pi}g(\nu, x)\mathcal{A}_{ki} \quad (1)$$

where $g(\nu, x)$ is the normalized (with respect to the frequency) lineshape and $g_k$ ($g_i$) is the degeneracy of the upper (lower) level. The integral of $\alpha(\nu, x)$ over the length $\ell$ of the absorption cell can be measured from the frequency-dependent vapor transmission $T(\nu)$:

$$T(\nu) \equiv \frac{P_t(\nu)}{P_0(\nu)} = \mathrm{e}^{-\int_0^\ell \alpha(\nu,x)\mathrm{d}x} \quad (2)$$

where $P_0$ and $P_t$ indicate the laser power before and after the cell respectively. The ratio between the integrated absorption coefficients of the two lines is independent on $N(x)$ and $\ell$:

$$\frac{\left[\int \mathrm{d}\nu \int \mathrm{d}x\alpha(\nu, x)\right]_{^3P_1 \to {}^1S_0}}{\left[\int \mathrm{d}\nu \int \mathrm{d}x\alpha(\nu, x)\right]_{^1D_2 \to {}^1S_0}} = \frac{\left[\frac{g_k}{g_i}\frac{\lambda^2}{4\pi}\mathcal{A}_{ki}\int \mathrm{d}xN(x)\int \mathrm{d}\nu g(\nu, x)\right]_{^3P_1 \to {}^1S_0}}{\left[\frac{g_k}{g_i}\frac{\lambda^2}{4\pi}\mathcal{A}_{ki}\int \mathrm{d}xN(x)\int \mathrm{d}\nu g(\nu, x)\right]_{^1D_2 \to {}^1S_0}} = \frac{1}{3}\left(\frac{657.3}{457.5}\right)^2 \frac{\mathcal{A}_{^3P_1 \to {}^1S_0}}{\mathcal{A}_{^1D_2 \to {}^1S_0}}\frac{g_{^3P_1}}{g_{^1D_2}} \quad (3)$$

where the factor $\frac{1}{3}$ arises from the three-pass geometry for the blue beam in our apparatus. Our measurements were made in the linear absorption regime, *i.e.* we checked that saturation effects were absent (see also further discussion).

To measure the integrated absorption we simultaneously scanned the two lasers across the lines, and fitted the recorded profiles assuming a pure Doppler line broadening (Fig. 3). In fact, the ratio between Doppler and homogeneous line-width is expected to be of the order of $10^3$.

For an exact interpretation of the recorded data it is necessary to take into account the isotopic structure of the absorption line, which is different for the two transitions. We considered the three most abundant isotopes of Ca ($^{40}$Ca, isotopic abundance 96.941%, $^{44}$Ca, isotopic abundance 2.086%, and $^{42}$Ca, isotopic abundance 0.647%) and the values of the isotope shifts available in literature. For the intercombination line, the experimental values in [22] were used: the shifts for the 40-42 and 40-44 pairs are respectively 509.5 and 996.2 MHz. This causes an asymmetry in the Doppler-broadened absorption profile that can be put on evidence in the experimental data (see Fig. 4). For the $E2$ line no experimental values are available for the isotope shifts. From the data in [22] we have however done a theoretical estimation of 3.5 GHz and 1.8 GHz respectively for the 40-44 and 40-42 pairs. The peak of $^{44}$Ca then falls outside of the scanning range of our laser, thus reducing the systematic error due to the inaccuracy of our estimation. In fact, for the $E2$ line no line asymmetries were observed in our experiment.

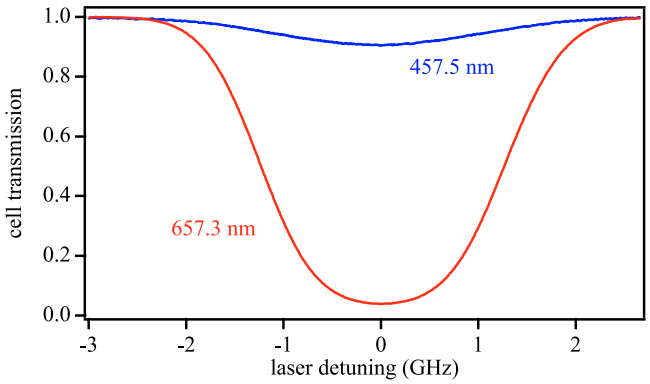


**Fig. 3.** Typical experimental absorption profiles.

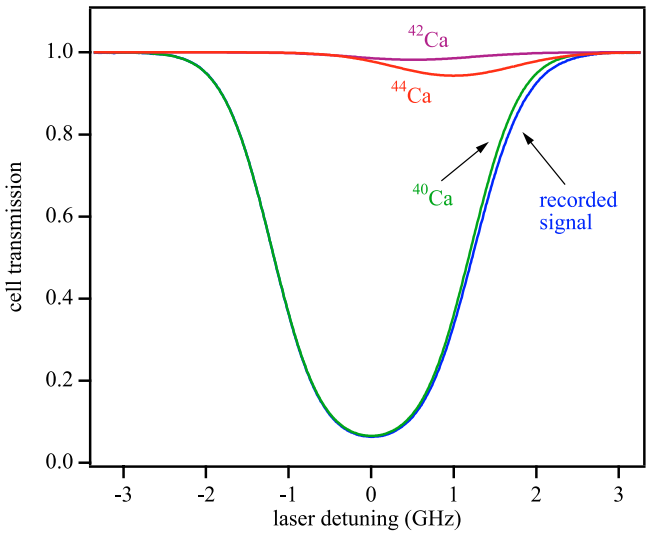


**Fig. 4.** Isotopic structure of the intercombination line; the absorption profile due to each isotopic component is shown, as deduced from our fit, together with the recorded signal. The fitted curve (Eq. (4) in the text) is indistinguishable from the recorded signal on this scale.

The numerical analysis was made in the following way. We fitted the recorded absorption profiles, that is, the ratio between the signal $S_t(\nu)$ of the photodiode after the cell and the signal $S_n(\nu)$ of the intensity-normalization photodiode, to the function

$$\frac{S_t(\nu)}{S_n(\nu)} = A\mathrm{e}^{-B\bar{g}(\nu)} \quad (4)$$

assuming for the normalized line-shape $\bar{g}(\nu)$ the form

$$\bar{g}(\nu) = 0.96941G(\nu) + 0.02086G(\nu - \Delta\nu_{40-44}) + 0.00647G(\nu - \Delta\nu_{40-42}) \quad (5)$$

where $\Delta\nu_{40-44}$ and $\Delta\nu_{40-42}$ are the isotopic transition frequency shifts and $G(\nu)$ is the normalized Gaussian function, centered at the resonance frequency $\nu_{40}$ for the $^{40}$Ca isotope:

$$G(\nu) = \frac{2}{\delta\nu}\sqrt{\frac{\ln 2}{\pi}}\mathrm{e}^{-\frac{4\ln 2(\nu-\nu_{40})^2}{\delta\nu^2}}. \quad (6)$$

The validity of our procedure relies on the principle of spectral stability, equation (1). That is, the frequency integral of the absorption coefficient is independent on the line broadening mechanisms. Equation (1) is true as long as the saturation parameter of the line is low compared to 1. This condition is well satisfied in our experiment. The saturation parameter is given by

$$S = \frac{IB_{ik}}{c\Gamma} \quad (7)$$

where $I$ is the laser intensity, $\Gamma$ is the homogeneous linewidth, $c$ is the speed of light and $B_{ik}$ is the Einstein $B$ coefficient of the transition. The line broadening due to the finite interaction time with the laser beams is of the order of few hundreds of kHz for both lines, while the pressure broadening is of $1.5 \div 3$ and $1 \div 2$ MHz for the red and the blue line respectively (see Sect. 2.5). Thus the homogeneous linewidth is dominated by collision broadening in our experiment, and the saturation parameter turns out to be of the order of $10^{-2}$ for the red line and of the order of $2 \times 10^{-5}$ for the blue line. In any case we have experimentally verified that no saturation effect is visible by changing the intensities of the light beams.

By fitting the recorded profiles as in equation (4) we have assumed that

$$\frac{\int \mathrm{d}x N(x) g(\nu, x)}{\int \mathrm{d}x N(x)} = \bar{g}(\nu) \quad (8)$$

but this may not be true, even if $g(\nu, x) = \bar{g}(\nu)\ \forall x$, as the temperature is not uniform along the cell. However, the quality of our fits was quite satisfactory (see Fig. 4). Thus the fit provided a precise estimation of the integral of the absorption coefficient, which is the aim of our measurement.

The Doppler linewidth $\delta\nu$ as deduced from the fit gives an independent estimation of an "effective" vapor temperature. As a test for the consistence of our procedure, we compared the observed line-widths of the two simultaneously recorded profiles (at 657.3 nm and 457.5 nm). We found a value of $1.00 \pm 0.01$ for the ratio between the relative line-widths.

We obtained the integrated absorption coefficient as the parameter $B$ of the fit; then we applied (3) to deduce the ratio between the transition rates. We repeated the procedure several times on different days, varying the cell temperature and the buffer gas pressure in order to change the absorption length and the optical beam alignment too. Due to the high ratio between the absorption coefficients of the two lines, the chosen values of the atomic density had to be a compromise between a significant absorption for the blue radiation and an observable transmission for the red radiation. The results are summarized in Figure 5.

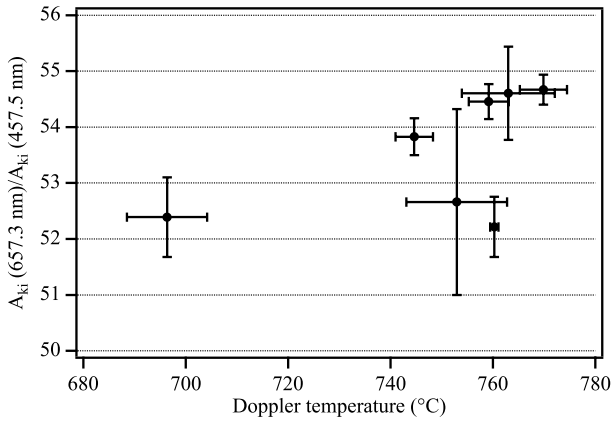


**Fig. 5.** Measured ratio between the $^1S_0 \rightarrow {}^3P_1$ and $^1S_0 \rightarrow {}^1D_2$ transition rates; each point represents a group of measurements, taken under different conditions of pressure, temperature and optical beam alignment. The horizontal scale is the Doppler temperature $\delta\nu$ as deduced from the fit on the intercombination line; the error bars are the standard deviations in each group.

We measured the ratio between the two transition rates as $(54.1 \pm 2.4)$. The uncertainty on our result is given by the combination of a statistical uncertainty (1.7%), given by the spread of the different measurements, and of an estimate (4.1%) for the systematic uncertainty. Possible sources of systematic uncertainty are the calibration system for the frequency scale (0.6%), and the inaccuracy of the isotope shift determination on the $E2$ line (0.4%).

The strongest contribution to systematic uncertainty comes from the possible presence of spectral impurities and small irregularities in the laser spectral scanning. We estimate this effect to be of the order of 4%, as deduced from the spread of the experimental results observed in some scanning (not considered in the statistical analysis) in which the red laser presented a higher level of spectral noise.

Considering the value of $(0.34 \pm 0.02)$ ms for the $^3P_1$ lifetime [15], we give an estimation of $(54.4 \pm 4.0)\ \mathrm{s}^{-1}$ for the $E2$ transition rate.

## 4 Conclusions

The precision of our estimation of the $E2$ transition rate is limited by the uncertainty (6%) on the value of the $^3P_1$ lifetime [15].

Our result is significantly higher than the value reported in reference [8]. We cannot give an explanation for this; however we can consider that in reference [8] the

measurement was performed at a much higher Ca density and buffer gas pressure, using a white light source. The calibration of the Ca density was made in comparison with the 422.7 nm resonance transition, using the hook method. The derivation of the oscillator strength value of the $^1S_0 \rightarrow ^1 D_2$ $E2$ transition (and then also of the transition probability $\mathcal{A}_{ki}$) in reference [8], is then less straightforward than our procedure and it may be more sensitive to perturbing factors.

We thank Mr M. Francesconi for the precious technical help provided. This work has been partially supported by INTAS programs.

## References

1. C.W. Oates, M. Stephens, L. Hollberg, in *Proceedings of the 1997 IEEE International Frequency Control Symposium* (IEEE, New York, NY, USA, 1997), p. 219
2. F. Riehle, H. Schnatz, B. Lipphardt, G. Zinner, T. Trebst, J. Helmcke, IEEE Trans. Instr. Meas. **48**, 613 (1999)
3. P. Kersten, F. Mensing, U. Sterr, F. Riehle, Appl. Phys. B **68**, 27 (1999)
4. K.R. Vogel, S.A. Diddams, C.W. Gates, E.A. Curtis, R.J. Rafac, W.M. Itano, J.C. Bergquist, W. Fox, W.D. Lee, J.S. Wells, L. Hollberg, Opt. Lett. **26**, 102 (2001)
5. S.N. Bagayev, V.I. Baraulya, A.E. Bonert, A.N. Goncharov, M.R. Seydaliev, Opt. Commun. **196**, 201 (2001)
6. F. Ruschewitz, J.L. Peng, H. Hinderthur, N. Schaffrath, K. Sengstock, W. Ertmer, Phys. Rev. Lett. **80**, 3173 (1998)
7. R. Drozdowski, J. Kwela, M. Walkiewicz, Z. Phys. D **27**, 321 (1993)
8. K. Fukuda, K. Ueda, J. Phys. Chem. **86**, 676 (1982)
9. L. Pasternack, D.R. Yarkony, P.J. Dagdigian, D.M. Silver, J. Phys. B **13**, 2231 (1980)
10. R.N. Diffenderfer, P.J. Dagdigian, D.R. Yarkony, J. Phys. B **14**, 21 (1981)
11. C.W. Bauschlicher Jr, S.R. Langhoff, H. Partridge, J. Phys. B **18**, 1532 (1985)
12. D.R. Beck, C.A. Nicolaides, J. Phys. B **16**, L627 (1983)
13. N. Vaeck, M. Godefroid, J.E. Hansen, J. Phys. B **24**, 361 (1991)
14. Y.G. Yi *et al.*, Acta Phys. Sin.-Ch. Ed. **50**, 37 (2001)
15. R. Drozdovski, M. Ignaciuk, J. Kwela, J. Heldt, Z. Phys. D **41**, 125 (1997)
16. F. Biraben, Opt. Commun. **29**, 353 (1979)
17. G.D. Boyd, D.A. Kleinman, J. Appl. Phys. **39**, 3597 (1968)
18. O.S. Brozek, V. Quetschke, A. Wicht, K. Danzmann, Opt. Commun. **146**, 141 (1998)
19. C.E. Wieman, L. Holberg, Rev. Sci. Instrum. **62**, 1 (1991)
20. K.B. MacAdam, A. Steinbach, C. Wienman, Am. J. Phys. **60**, 12 (1992)
21. J. Rohe-Hansen, V. Helbig, J. Phys. B **25**, 71 (1992)
22. E. Bergmann, P. Bopp, Ch. Dorsch, J. Kowalski, F. Träger, Z. Phys. A **249**, 319 (1980)
23. A. Aspect, J. Bauchet, M. Godefroid, P. Grangier, J.E. Hansen, N. Vaeck, J. Phys. B **24**, 4077 (1991)